#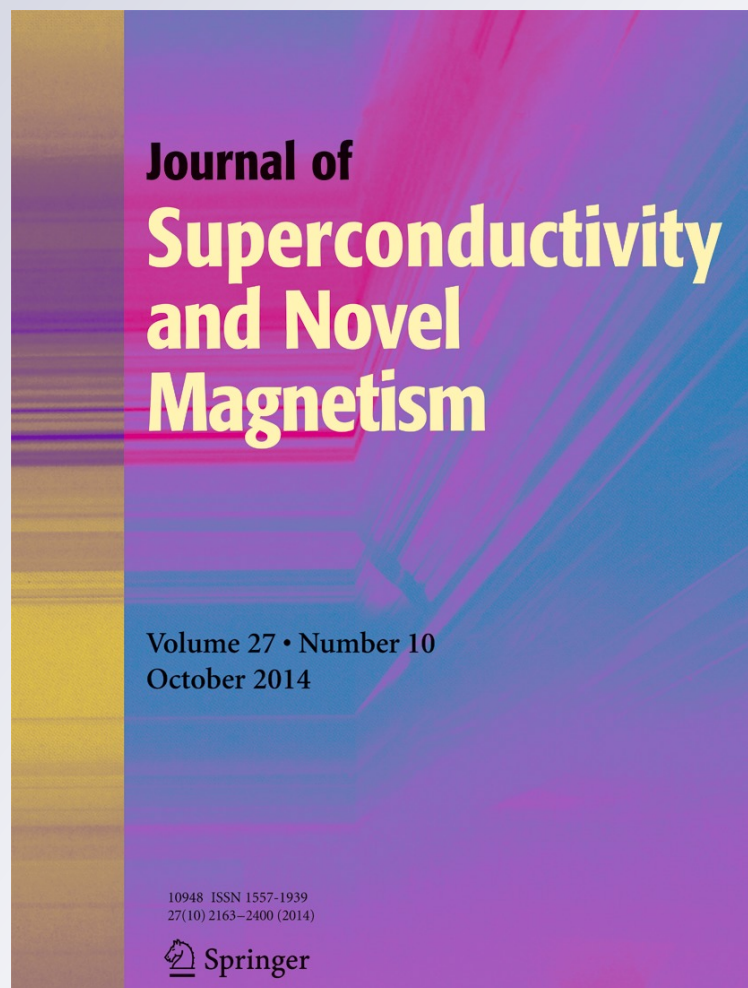 Critical Current Density and Intergranular Coupling Study of the Dysprosium Oxide Nanoparticle Added $Bi_{1.6}Pb_{0.4}Sr_2Ca_2Cu_3O_y$ Superconductor

A. Zelati, A. Amirabadizadeh, A. Kompany, H. Salamati & J. E. Sonier

Springer

Springer

ORIGINAL PAPER

Critical Current Density and Intergranular Coupling Study of the Dysprosium Oxide Nanoparticle Added $Bi_{1.6}Pb_{0.4}Sr_2Ca_2Cu_3O_y$ Superconductor

A. Zelati · A. Amirabadizadeh · A. Kompany · H. Salamati · J. E. Sonier

Abstract The dysprosium oxide nanoparticles' addition effects on structural, DC electrical resistivity, critical current density, and AC magnetic susceptibility properties of polycrystalline $Bi_{1.6}Pb_{0.4}Sr_2Ca_2Cu_3O_y$ samples are investigated. X-ray diffraction (XRD) analysis showed that both (Bi,Pb)-2223 and Bi-2212 phases coexist in the samples having orthorhombic crystal structure. Bi-2223 phase concentration increases with increasing dysprosium nanoparticle concentration. DC electrical resistivity, critical current density (J_c), and AC susceptibility measurements reveal that adding dysprosium nanoparticles to bismuth–strontium–calcium–copper–oxide (BSCCO) improves superconducting properties of this system and enhances its critical current density due to the improvement of the grain connectivity with dysprosium nanoparticle addition.

A. Zelati (✉) · A. Amirabadizadeh
Department of Physics, University of Birjand,
Birjand, 97175/615, Iran
e-mail: a_zelati@yahoo.com; azellati@birjandut.ac.ir

A. Kompany
Department of Physics, Ferdowsi University of Mashhad,
Vakilabad Hwy, Mashhad, 9177948974, Iran

H. Salamati
Faculty of Physics, Technology University of Isfahan,
Daneshgah e Sanati HW, Isfahan, 8415683111, Iran

J. E. Sonier
Department of Physics, Simon Fraser University,
Burnaby, BC, V5A 1S6, Canada

1 Introduction

Since the discovery of Bi-based superconducting systems, many studies have been devoted to improve their properties [1–3]. The bismuth–strontium–calcium–copper–oxide (BSCCO) system mainly contains three phases in the general formula $Bi_2Sr_2Ca_{n-1}Cu_nO_{2n+4+y}$ where $n = 1$, 2, and 3 refers to the number of CuO_2 layers which yield 10, 90, and 110 K superconducting phases, respectively [4]. The Bi-2201, Bi-2212, and Bi-2223 phases have single, double, and triple layers of CuO_2 in the subunit cell, respectively. Among these phases, the creation of Bi-2212 phase is thermodynamically stable over a large scale of temperature. Takano et al. have found that the partial lead substitution for bismuth could increase the volume fraction of Bi-2223 phase [5], but after more than two decades, the formation of pure Bi-2223 phase is still an open subject in the field of Bi-based superconductors [6–10].

In the application of BSCCO superconductors, higher critical current density (J_c) has a more significant role than the other factors. However, the major limitations of BSCCO superconductor applications are the intergrain weak links and weak flux pinning capability, which leads to weak critical current density in bulk samples. There have been remarkable improvements in enhancing transport properties of this high-critical temperature (T_c) superconductor, since BSCCO superconductor was discovered. We can enhance the superconducting properties of BSCCO system by addition or substitution of elements with different ionic radii and different bonding characters. As an example, to obtain

more applicable BSCCO sample, we can add or substitute metallic elements to the BSCCO system to improve the connectivity between grains leading to higher J_c [11]. Several researchers [12–16] have investigated the effects of rare earth oxides and some other oxide substitutions or additions on the superconducting and structural properties of BSCCO system. The works of most of these researches are related to addition or substitution of micro-oxide powders to BSCCO systems. With nanotechnology developments, a wide range of nanostructure materials has been synthesized. In the nanosize range, the particles have a high proportion of atoms located at its surface as compared to bulk materials, giving rise to unique physical and chemical properties that are very different from their bulk counterparts [17]. In recent years, studying the effects of nanoparticle addition or substitution to BSCCO system has been of much interest [18–21]. When nanoparticles are added to the BSCCO system, due to the tiny size of nanoparticles, they settle easier and much more among the grains of these ceramic superconductors than the microsize dopant. If an adequate amount of nanoparticles with metallic character is added to the BSCCO, the intergrain connectivity will possibly improve.

In this study, we added dysprosium oxide nanoparticles to the BSCCO system in order to improve the connectivity between grains. We generally expect that a small amount of dysprosium nanoparticle addition to BSCCO system would enhance the connectivity between grains due to metallic character of Dy or would make possible pinning centers between grain boundaries. The general formula for preparing the samples of this research was $Bi_{1.6}Pb_{0.4}Sr_2Ca_2Cu_3O_{y+x}Dy_2O_3$ and $x = 0.0, 0.3, 0.5,$ and 1.0 wt%. To the best of our knowledge, the previous studies on effects of Dy on BSCCO system were related to the microsize of dysprosium powder and were focused on magnetic properties. Berger et al. [16] studied the coexistence of ferromagnetism and high-T_c superconductivity in micron doping of Dy on BSCCO system, but the structural effect of this dopant and the effects of Dy nanoparticle addition on the superconducting properties of BSCCO system have been left untouched. The BSCCO sample was prepared by chemical sol-gel method [22–25] and Dy_2O_3 nanopowder by combustion method. The methods used in analyzing data and results are given in the following sections.

2 Experimental

2.1 Sample Preparation

The samples were prepared according to the general formula $Bi_{1.6}Pb_{0.4}Sr_2Ca_2Cu_3O_{y+x}Dy_2O_3$ and $x = 0.0, 0.3, 0.5,$ and 1 wt% on three steps as follows.

2.1.1 BSCCO Preparation

BSCCO sample with chemical composition $Bi_{1.6}Pb_{0.4}Sr_2Ca_2Cu_3O_y$ was prepared by chemical sol-gel method, using the powders of $Bi(NO_3)_2 \cdot 5H_2O$, $Pb(NO_3)_2$, $Sr(NO_3)_2$, $Ca(NO_3)_2 \cdot 4H_2O$, and $Cu(NO_3)_2 \cdot 3H_2O$ as starting materials. EDTA with chemical composition $N_2H_{10}O_{16}$ was used as a complexing agent with the molar ratio EDTA/cation $= 1$, ethylene glycol (EG) with chemical composition $C_2H_4(OH)_2$ as a binding agent of complexes with a molar ratio EG/cation $= 3$, and urea as a fuel with a molar ratio urea/cation $= 0.7$. Distilled water and nitric acid were used as a solvent. Bismuth nitrate was poured in an appropriate volume of distilled water (400 mL for 40 gr final production) at temperature 40 °C. The certain amount of nitric acid was added to the mixture to make the bismuth solution. Then, the other nitrates were added to this solution. After stirring the mixture, a transparent blue solution with pH $= 1$ was obtained, which we named the material solution. After that, the certain amount of EG was solved in an appropriate volume of distilled water (400 mL for 50 gr final production) at temperature 40 °C, and then, EDTA was added to this solution which resulted in the formation of precipitation. In order to annihilate the precipitation, NH_3OH was added to the liquid mixture so that a transparent solution with pH $= 6$ was obtained (main solution). The material solution was poured into the main solution drop by drop at temperature 60 °C until formation of precipitation starts. At this time, the process of adding the material solution to the main solution was stopped to eliminate the precipitation via NH_3OH. This process was repeated until all the material solutions were added to the main solution, obtaining the gel with pH $= 4$. The next performance was adding urea as the fuel to the prepared gel. Then, the urea-added gel was dried on a hot plate with a gradually increasing temperature from 60 to 200 °C, which took 3 days to complete the process of drying. At the end of this time, a rather weak combustion occurred, and a gray color powder was produced. The powder was grinded and calcined at 850 °C for 7 h in air. After calcination, a black powder was obtained. The prepared powder was then grinded and divided in four segments.

2.1.2 Nanoparticle Preparation

Dy_2O_3 nanoparticles were prepared by combustion method using dysprosium(III) nitrate pentahydrate with chemical composition $Dy(NO_3) \cdot 5H_2O$ as a starting material. Distilled water was used as the solvent and glycine with chemical formula $C_2H_5NO_2$ as the fuel of the reaction. Dysprosium(III) nitrate pentahydrate was solved in an adequate amount of distilled water. After obtaining aqueous solution of cation, Dy^{3+}, glycine as the fuel for combustion was

added to the solution. The liquid mixture was placed inside the preheated (300 °C) oven for 1 h. Combustion took place inside the oven, and russet smoke of the NO_2 gas came out. The resultant product was a voluminous, foamy white powder. Later, X-ray diffraction (XRD) pattern and TEM images confirmed the cubic structure and the nanosize of the prepared Dy_2O_3 powder.

2.1.3 Nanoparticle Preparation

Dy_2O_3 nanopowder, in this step, was added to each of segments (1, 2, 3, and 4) prepared in the first step with 0.0, 0.3, 0.5, and 1.0 wt%, respectively. Each sample was grinded and calcined at 850 °C for 7 h in air. The calcined powders were grinded again and pressed under 450 MPa pressure to form pellets with 11 mm diameter and 3.5 mm thickness. The prepared pellets were finally sintered at 860 °C for 24 h in air. Sample with $x = 0.0$ in general chemical formula, $Bi_{1.6}Pb_{0.4}Sr_2Ca_2Cu_3O_{y+x}Dy_2O_3$, was labeled as sample A, and the other samples labeled as B ($x = 0.3$), C ($x = 0.5$), and D ($x = 1.0$).

2.2 Sample Characterization

XRD and SEM were used for the structural studies of the samples. DC resistivity, J_c, and AC magnetic susceptibility measurements were carried on to study the superconducting properties of the samples. The X-ray powder diffraction pattern for each sample was obtained using CuKα (1.54 Å) radiation in the range $2\theta = 20 - 65°$ using a Rigaku R-Axis Diffractometer. Phase purity and the lattice parameters were obtained from these patterns. SEM imaging was used to examine the surface morphology and grain structure of the samples. SEM images were taken by using a Strata Dual Beam 235 field emission scanning electron microscope. The R–T behavior of the samples from 30 K to room temperature was investigated in order to determine the superconducting transition temperature. The electrical resistance measurements and J_c determination were performed using the standard four-probe method. The magnetic susceptibility measurements carried out employing a Quantum Design SQUID magnetometer MPMS-XL7 that works between 1.8 and 400 K with a 7T superconducting magnet. Diamagnetic corrections were applied for the sample holder and the core diamagnetism of the samples.

3 Results and Discussion

3.1 Structural Studies

XRD patterns of $Bi_{1.6}Pb_{0.4}Sr_2Ca_2Cu_3O_{y+x}D_2O_3$ ($x = 0.0$, 0.3, 0.5, and 1.0 wt%) samples indicated that all samples

consist of two phases: Bi-2212 and Bi-2223 phases with 2223 phase being the dominant one (Fig. 1). To estimate the volume fraction of the present phases, we used the corresponding Bi-2212 and Bi-2223 peaks and the following formulas [18]:

$$\text{Bi-(2223)}\% = \frac{\Sigma I(2223)}{\Sigma I(2223) + I(2212)} \times 100$$

$$\text{Bi-(2212)}\% = \frac{\Sigma I(2212)}{\Sigma I(2223) + I(2212)} \times 100$$

where $I(2223)$ and $I(2212)$ are the intensities of the (hkl) XRD peaks for Bi-2223 and Bi-2212, respectively. The calculated relative portions of each phase of the samples are listed in Table 1. As seen in the table, samples with $x = 0.0$, 0.3, 0.5, and 1.0 contained 76, 78.5, 80, and 68 % of the 2223 phase, respectively.

The concentration of 2223 and 2212 phases as a function of x evaluated from XRD patterns of $Bi_{1.6}Pb_{0.4}Sr_2Ca_2Cu_3O_{y+x}Dy_2O_3$ ($x = 0.0$, 0.3, 0.5, and 1.0) samples are given in Fig. 2. It is seen that the volume fraction of the Bi-2223 phase increases with increasing dysprosium nanoparticle concentration up to $x = 0.5$, while a decrease in the volume fraction of the Bi-2223 phase was observed for sample D ($x = 1$ wt%).

The crystal system of Dy-free sample was found to be orthorhombic with the lattice parameters of $a = 5.315$ Å, $b = 5.419$ Å, and $c = 37.298$ Å. Almost, the same lattice parameters were obtained for the Dy nanoparticle-added samples. The results are given in Table 1. There is no distortion in the crystal system of the Dy-added Bi-2223, which shows that Dy particles do not participate in the crystal structure of the Bi-2223. We believe that the added nanoparticles are sited between the superconducting grains. The role of such impurity nanoparticles either can be as the pinning centers to fix vortices or may enhance connectivity between grains, which may lead to higher J_c [11].

Figure 3 displays the surface SEM images of the Dy nanoparticle-free and Dy nanoparticle-added samples. It is observed that the microstructures of all samples exhibit a common feature of plate-like grains and are randomly distributed. We believe that white particles sited between the grains are dysprosium nanoparticles, which are obvious in the micrographs of dysprosium-added samples. These particles can enhance the connectivity among the grains, and they can increase the pinning centers to fix the vortices. SEM results corroborate well with XRD results. Grain size of sample D decreases compared to that of the other samples, which may cause a decrease in superconducting properties of this sample.

The theoretical density of BSCCO system is about 6.3 g cm^{-3} obtained from the lattice parameters [26]. The density of pellets in this work was determined as 5.48, 5.21, 5.19, and 4.88 g cm^{-3} for $x = 0.0$ to $x = 1.0$, respectively,
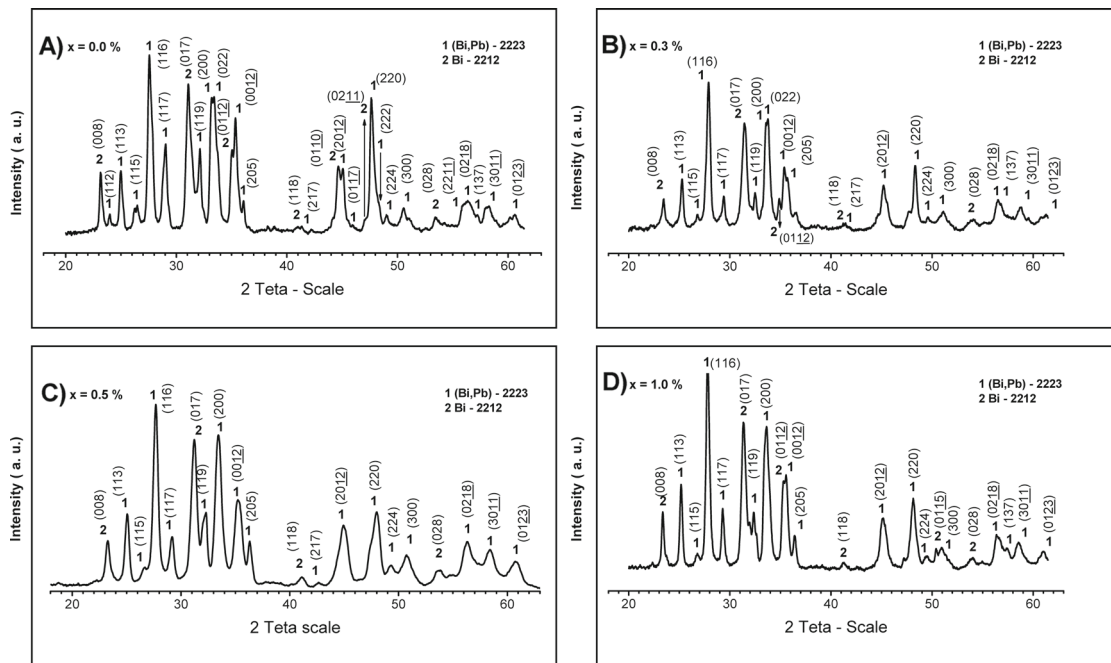
Fig. 1 XRD patterns of $Bi_{1.6}Pb_{0.4}Sr_2Ca_2Cu_3O_{y+x}Dy_2O_3$ samples. Peaks of 2223 and 2212 phases are indexed *1* and *2*, respectively

measured by water displacement Archimedes' method. The bulk densities obtained by the Archimedes technique is in the range of 78 to 87 % of the theoretical values. This result is in accordance with the porous structure of ceramic superconductors.

3.2 Superconducting Properties Measurements

As shown in Fig. 4, DC electrical resistance reveals that the resistivity of the presented samples decrease linearly with temperature in the normal state. All samples displayed a metallic character above onset temperature, which is defined as the temperature where *R–T* plot deviates from linearity [10]. Derivatives of the *R–T* curves were calculated to obtain the zero onset transition to the superconducting state. The plots of the samples have a shoulder, which we believe to be due to the coexistence of Bi-2223 and Bi-2212 phases. The onset critical temperature ($T_{c,onset}$) and the zero resistivity critical temperature ($T_{c,R=0}$) of the samples are tabulated in Table 2.

As seen in the table, $T_{c,\,onset}$ of the samples A, B, and C is 109.5 K, and for sample D, it is 107 K. It is seen that $T_{c,\,R=0}$ shifts to higher temperatures with increasing Dy nanoparticle concentration up to $x = 0.5$, and the transition temperature width (ΔT_c) decreases, implying an enhancement in the intergrain connectivity [11]. However, for the sample D ($x = 1.0$), $T_{c,R=0}$ shifts to lower temperature compared to Dy-free sample, and since, in sample D, $T_{c,\,onset}$ also is lower than that in sample A, at this stage, we cannot conclude that for this sample, improvement or destruction has occurred in the intergrain connectivity. The variation of T_c with Dy content, x, is given in Fig. 5.

A parabolic relationship holds between the superconducting transition temperature and the hole concentration. The hole concentration is calculated using the relation given below [27]:

$$p = 0.16 - \left[(1 - T_c/T_c^{max})/82.6\right]^{1/2}$$

where p indicates hole concentration, and T_c^{max} is taken as 110 K for the Bi-2223 system. Previous calculations for

Table 1 The lattice parameters and volume fraction of Bi-2223 and Bi-2212 phases in $Bi_{1.6}Pb_{0.4}Sr_2Ca_2Cu_3O_{y+x}Dy_2O_3$ samples

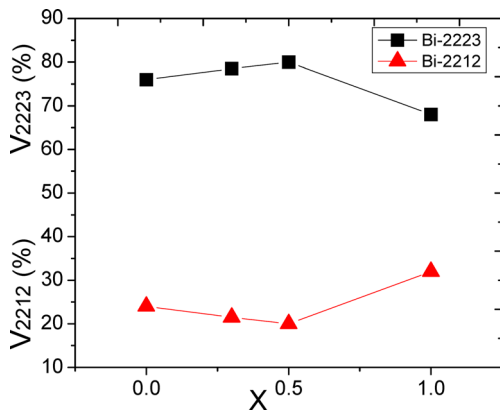| Sample	Dy (x)	Orthorhombic unit cell (Bi-2223 phase)			Volume fraction of phase formed (%)	
		a (Å)	b (Å)	c (Å)	Bi-2223 phase	Bi-2223 phase
A	0.0	5.315	5.419	37.298	76	24
B	0.3	5.317	5.418	37.285	78.5	21.2
C	0.5	5.321	5.417	37.292	80	20
D	1.0	5.307	5.422	37.271	68	32

Fig. 2 Volume fraction of Bi-2223 and Bi-2212 phases determined from XRD patterns

the unsubstituted Bi-2223 had shown that the values of p are in the range of 0.116 to 0.160 [27]. Figure 6 shows the critical temperature versus hole concentration plot. Hole carrier concentration varies from 0.1016 for Dy-free sample to 0.1065 for sample C ($x = 0.5$). The hole concentration increases with increasing Dy nanoparticle concentration up to $x = 0.5$. However, for sample D with $x = 1.0$, the hole concentration starts to decrease to lower amounts.

The critical current density of the samples was measured at a temperature of 77 K in zero magnetic field as shown in graphs of current density versus voltage in Fig. 7. J_c values of the samples are given in Table 2. According to the results, an enhancement in the critical current density of the Dy nanoparticle-added samples is observed, which is proportional to the concentration of the Dy in the samples B and C ($x = 0.3$ and 0.5), but not for sample D. This improvement in J_c may be attributed to the enhancement in the intergrain connectivity.

AC susceptibility measurement ($\chi' + i\chi''$) is widely used as a nondestructive method for determination and characterization of the intra- and intergrain features of the high temperature superconductors. The in-phase component of fundamental susceptibility, χ', shows two significant drops as the temperature is decreased below T_c for granular superconductors. The sharp drop, near T_c, corresponds only to the intrinsic properties of the grains. Another drop at low temperatures indicates gradual changes associated with the occurrence of bulk superconductivity, where there is superconducting current flow from grain to grain. The out-of-phase component, χ'', generally exhibits a peak with a decreasing temperature below T_c, which is attributed to the absorption of magnetic energy of the superconductor from

Fig. 3 SEM surface micrographs of $Bi_{1.6}Pb_{0.4}Sr_2Ca_2Cu_3O_{y+x}Dy_2O_3$ samples. **a** $x = 0.0$ wt%, **b** $x = 0.3$ wt%, **c** $x = 0.5$ wt%, and **d** $x = 1.0$ wt%
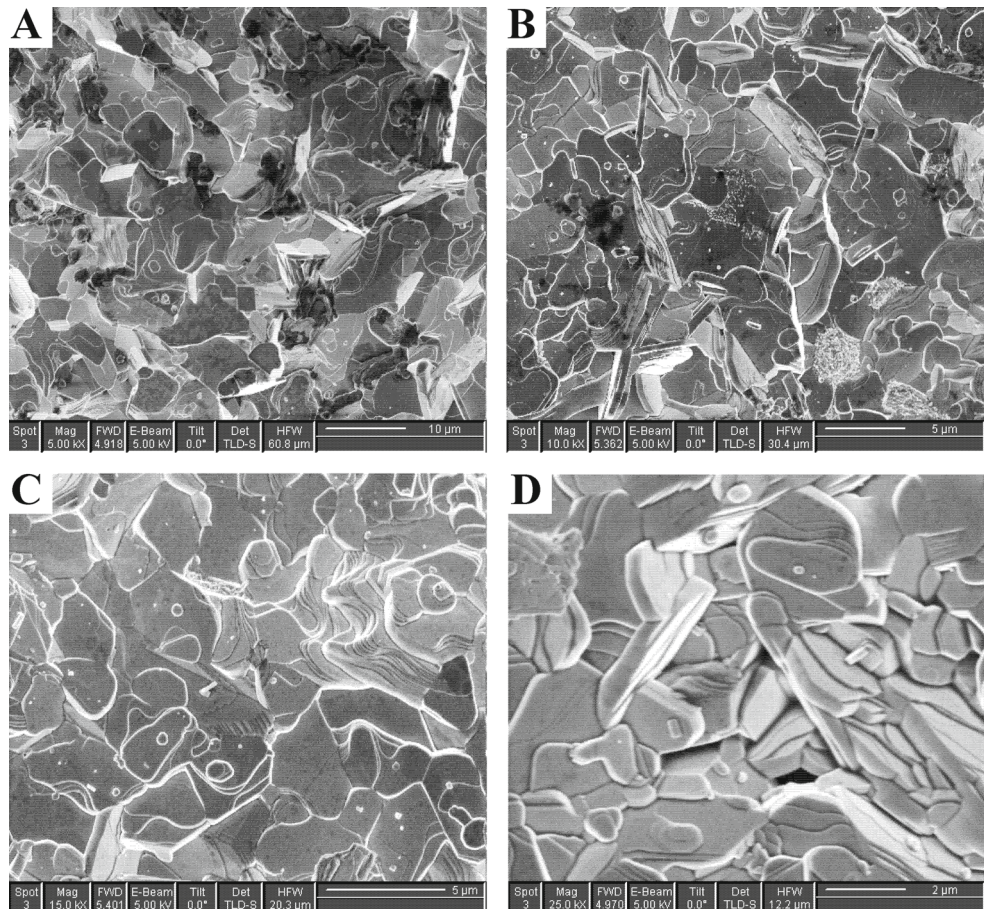
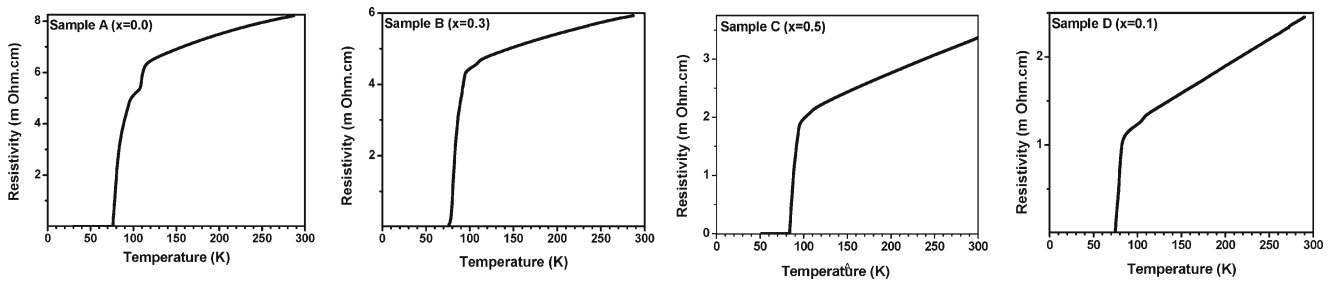**Fig. 4** Temperature dependences of the electrical resistivity for $Bi_{1.6}Pb_{0.4}Sr_2Ca_2Cu_3O_{y+x}Dy_2O_3$ samples

Table 2 The critical temperatures, mass density, and critical current density of dysprosium-free and dysprosium-added samples

Sample	Dy (x)	$T_{c, onset}$ (K)	$T_{c, R=0}$ (K)	ΔT_c (K)	Mass density (g cm^{-3})	J_c (A cm^{-2})
A	0.0	108	79	29	5.48	15.90
B	0.3	108	81	27	5.21	18.32
C	0.5	108	84	24	5.19	20.11
D	1.0	105	80	26	4.88	13.05

the AC field. Therefore, χ' is proportional to an amount of flux penetration into the body of the superconductor, while χ'' is associated with AC losses in the mixed state of superconductor [28].

In Fig. 8, the measurements of susceptibility versus temperature for Dy nanoparticle-free and Dy nanoparticle-added samples have been plotted for AC field of 80 A/m with $f = 330$ Hz. A broad magnetic transition for sample D ($x = 1.0$) is observed from measurement. Samples B ($x = 0.3$) and C ($x = 0.5$) have a slightly sharper transition compared to Dy-free sample. These results suggest that Dy nanoparticle-added samples up to $x = 0.5$ have better intergranular coupling between the grains, which is in good agreement with DC electrical resistivity and J_c measurements. It is seen that the peak in χ'' shifts to higher temperature with increasing dysprosium nanoparticle

concentration up to $x = 0.5$, while for sample D, the peak shifts to lower temperatures. This means that AC losses for dysprosium nanoparticle-added samples (up to $x = 1.0$) start at higher temperatures compared with Dy-free sample. The curve obtained from the derivation of χ' versus temperature is inserted in Fig. 8, displaying intra- and intergrain superconducting transition temperatures. The intragrain transition temperature was determined to be about 105 K for all samples. However, the intergrain transition temperature shows an increase directly proportional to dysprosium nanoparticle concentration starting from 85.5 K for Dy-free sample and reaching 89 and 91 K for samples B and C, respectively. For sample D, the value is 86 K, indicating a drop in the increase of the intergrain transition temperature.

Figure 9 shows the AC susceptibility curves of the samples measured in the presence of the three different magnetic
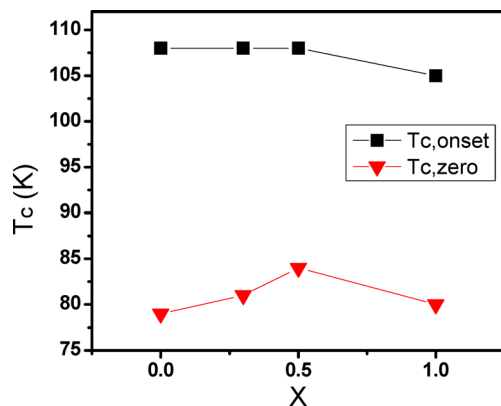

Fig. 5 Samples' critical temperature variation versus dysprosium nanoparticle concentration
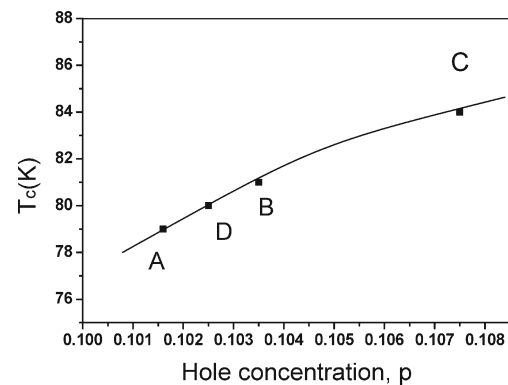

Fig. 6 Superconducting transition temperature versus hole concentration of dysprosium-free and dysprosium-added samples
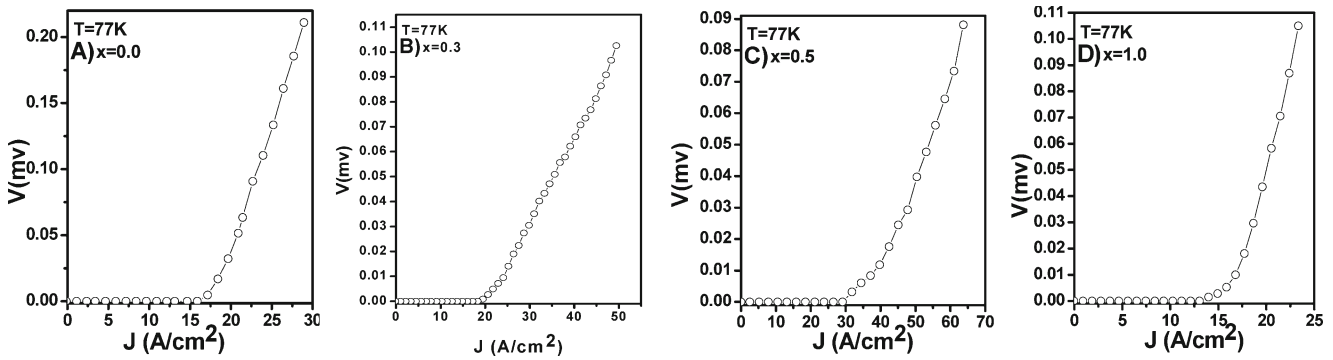
Fig. 7 Critical current density of the $Bi_{1.6}Pb_{0.4}Sr_2Ca_2Cu_3O_{y+x}Dy_2O_3$ samples
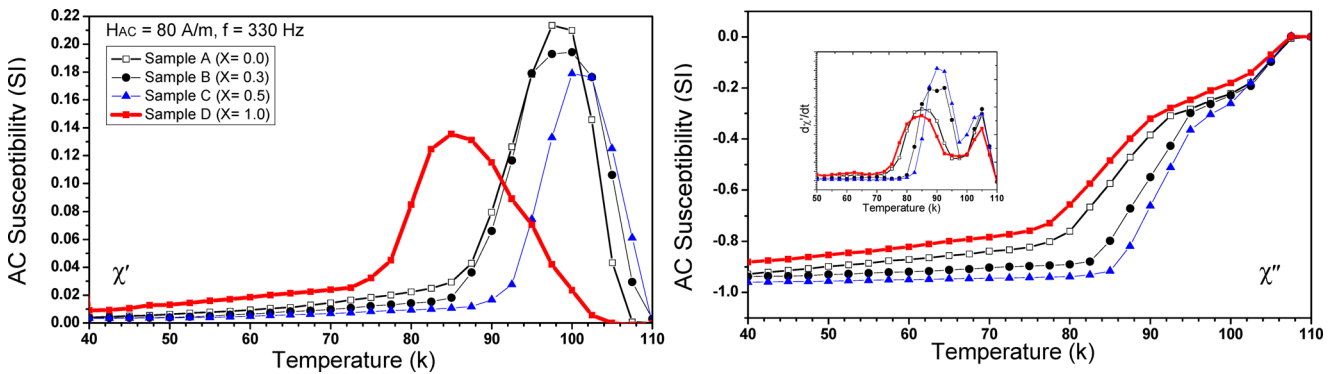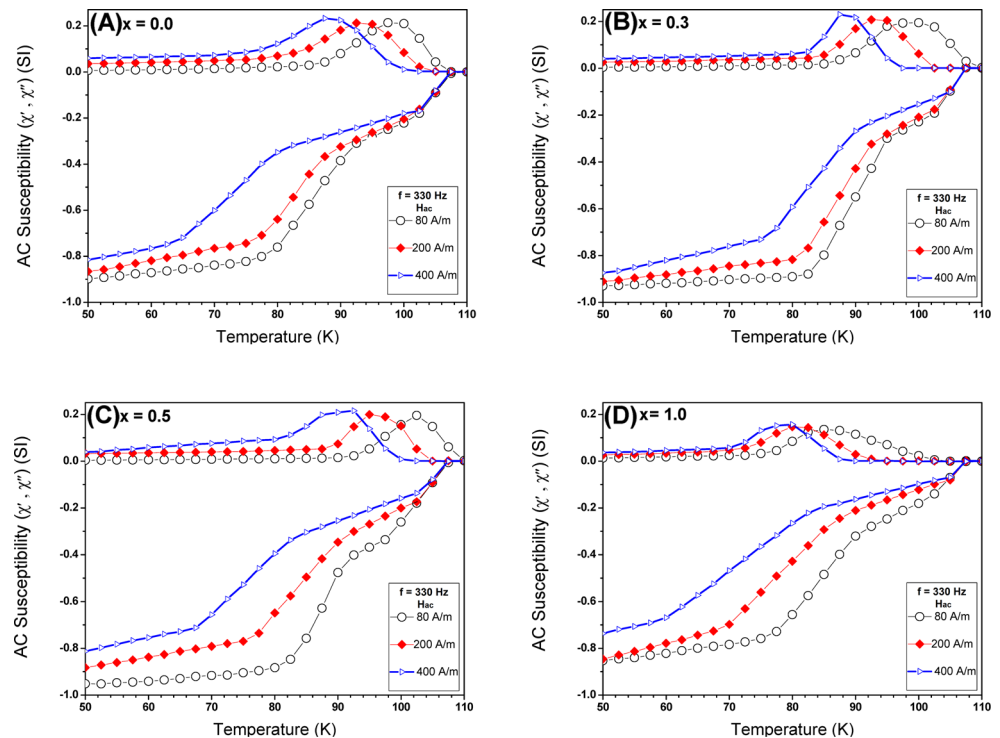

Fig. 8 AC magnetic susceptibility as a function of temperature for all samples. χ' Real part, χ'' imagery part. *Inset* indicates derivation of in-phase component versus temperature

Fig. 9 AC magnetic susceptibility of the samples as a function of temperature in the presence of different magnetic fields

fields. The diamagnetic onset temperature of the super-conducting transition is about 105 K for all samples. This temperature is independent of the applied field values for dysprosium nanoparticle-free and dysprosium nanoparticle-added polycrystalline samples and is in good agreement with DC resistivity measurements. It is well known that the minimum full flux penetration field, H_p, becomes larger by decreasing the temperature from T_c to the temperature T_p, at which χ'' peaks occur. The value of the measured AC field at these temperatures is sufficiently large enough to penetrate to the center of the sample. When $H_{AC} = H_p$, the full flux penetration occurs. A function of the form $H_p = H_{ac}(1 - t)^n$ fits best the data obtained, where $t = (T/T_c)$ is the reduced temperature. The function obtained thereby is employed as a scaling function for temperature sweep measurements, and it is most accurate at temperatures near T_c. By fitting H_{ac} versus $(1 - t)^n$ plot, we have found n for our samples. Figure 10 shows the temperature dependence of the intergranular critical current density, J_c, calculated from H_p values. According to Bean's model [28, 29], J_c at the peak temperature, T_p, can be calculated using the following relation:

$$J_c(T_p) = H_p / R \approx H_p \Big/ \sqrt{ab}$$

where $2a \times 2b$ is the cross section of the samples. It can be observed in Fig. 10 that there is the same behavior in increasing J_c for Dy nanoparticle-added samples in comparison with the Dy-free sample. The result of J_c measurements
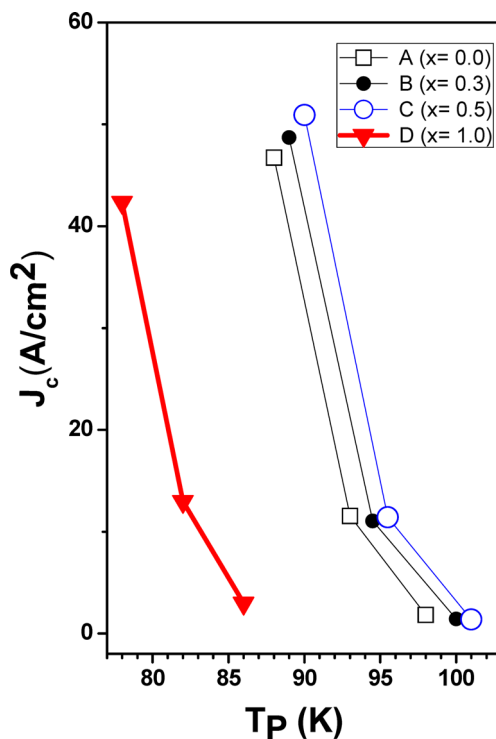
(Fig. 7) is in good agreement with the result of J_c calculated from H_p values (Fig. 10) in which this agreement reveals the most important feature of this study. The enhancement observed in J_c suggests that little amount ($x \leq 0.5$ wt%) of dysprosium nanoparticle addition may settle between grains and increase the connectivity of grains.

4 Conclusions

The samples with nominal composition $Bi_{1.6}Pb_{0.3}Sr_2$ Ca_2 $Cu_3 + xDy_2O_3$ ($x = 0.0, 0.3, 0.5,$ and 1.0 wt%) were prepared by the chemical sol-gel method. X-ray diffraction indicated that both Bi-2223 and Bi-2212 phases coexisted in the samples. The volume fraction, which was estimated by XRD peak intensities, showed an increase in the volume fraction of the Bi-2223 high-T_c phase with increasing dysprosium nanoparticle concentration up to $x = 0.5$ wt%. SEM results showed that the added dysprosium nanoparticles settled among the grain boundaries. $T_{c, onset}$ and $T_{c, R = 0}$ of all the samples were obtained from DC electrical resistivity measurements. Hole concentration of the samples, calculated by the results of DC measurements, showed an increase with increasing dysprosium nanoparticle concentration up to $x = 0.5$ wt%. Critical current density measurement showed an enhancement in the J_c values with increasing dysprosium nanoparticle concentration up to $x = 0.5$ wt%. Intergranular coupling, intra- and intergrain transition temperatures, and intergranular critical current density were calculated by AC magnetic susceptibility measurements. AC measurements demonstrated improvements in dysprosium-added samples. Based on observation, dysprosium nanoparticle addition up to $x = 0.5$ wt% improves intergrain connectivity which results in better superconducting properties of BSCCO system. Critical current density is enhanced with dysprosium nanoparticle addition.

Conflict of interest The authors declare that they have no conflict of interest.

Fig. 10 Variation of critical current density with temperature

References

1. Maeda, H., Tnaka, Y., Fukutomi, M., Asano A new, T.: High-T_c oxide superconductor without a rare earth element. Jpn. J. Appl. Phys. **27**, L209–L210 (1988)
2. Ozturk, O., Yegen, D., Yilmazlar, M., Varilci, A., Terzioglu, C.: The effect of cooling rates on properties of $Bi_{1.7}Pb_{0.35}Sr_{1.9}Ca_{2.1}$ Cu_3O_y superconductors produced by solid-state reaction method. Phys. C **451**, 113–117 (2007)

3. Michel, C., Hervieu, M., Borel, M.M., Grandin, A., Deslandes, F., Provost, J., Raveau, B.: Superconductivity in the Bi–Sr–Cu–O system. Z. Phys. B **68**, 421–423 (1987)

4. Gul, I.H., Rehman, M.A., Ali, M., Maqsood, A.: Effect of vanadium and barium on the Bi-based (2223) superconductors. Phys. C **432**, 71–80 (2005)

5. Takano, M., Takada, J., Oda, K., Kitaguchi, H., Miura, Y., Ikeda, Y., Tomii, Y., Mazaki, H.: High-Tc phase promoted and stabilized in the Bi,Pb-Sr-Ca-Cu-O system. Jpn. J. Appl. Phys. **27**, L1041 (1988). doi:10.1143/JJAP.27.L1041

6. Xi, Z., Ji, C., Zhou, L.: 112–114 K superconductors $Bi_{1.8}Pb_{0.3}$ $Sr_2Ca_2Cu_3O_y$ by means of a three-step reaction process. Solid State Commun. **72**, 1015–1017 (1989)

7. Zhigadlo, N.D., Petrashko, V.V., Semenenko, Yu.A., Panagopoulos, C., Cooper, J.R., Salje, E.K.H.: The effects of Cs doping, heat treatments on the phase formation and superconducting properties of (Bi,Pb)–Sr–Ca–Cu–O ceramics. Phys. C **299**, 327–337 (1998)

8. Gul, I.H., Anis-ur-Rehman, M., Maqsood, A.: Temperature dependence of thermal and electrical conductivity of Bi-based high-T_c (2223) superconductor. Phys. C **450**, 83–87 (2006)

9. Li, Y., Yang, B.: Doping of the Bi-Sr-Ca-Cu-O system with V_B elements and the effect on $Bi_2Sr_2Ca_2Cu_3O_y$ phase formation. J. Mater. Sci. Lett. **13**, 594–596 (1994)

10. Salamati, H., Kameli, P.: The effect of Bi-2212 phase on the weak link behavior of Bi-2223 superconductors. Phys. C **403**, 60–66 (2004)

11. Halim, S.A., Mohamed, S.B., Azhan, H., Khawaldeh, S.A., Sidek, H.A.A.: Effect of barium doping in Bi–Pb–Sr–Ca–Cu–O ceramics superconductors. Phys. C **312**, 78–84 (1999)

12. dos Santos, C.A.M., Mochlecke, S., Kopelevich, Y., Machado, A.J.S.: Inhomogeneous superconducting in $Bi_2Sr_2Ca_{1-x}Pr_x$ Cu_2O_{8-z}. Phys. C **390**, 21–26 (2003)

13. Rentschler, T., Kemmler-Sack, S., Hartmann, M., Hubenen, R.P., Kesselar, P., Lichte, H.: Influence of Nd substitution on the superconducting properties of ceramics in the 2212 system $Bi_{2-w}Pb_wSr_{2-y}Nd_{x+y}Cu_xO_{8+z}$. Phys. C **200**, 287–295 (1992)

14. Biju, A., Abhilash Kumar, R.G., Aloysius, R.P., Syamaprasad, U.: Structural and superconducting properties of $Bi_{1.7}Pb_{0.4}Sr_{2-x}Gd_x$ $Ca_{1.1}Cu_2O_y$. Phys. C **449**, 109–115 (2006)

15. Awana, V.P.S., Agarawal, S.K., Narlikar, A.V., Das, M.P.: Superconductivity in Pr- and Ce-Doped $Bi_2CaSr_2Cu_2O_y$ system. Phys. Rev. B **48**, 1211–1216 (1993)

16. Berger, H., Ariosa, D., Gaal, R., Saleh, A., Margaritondo, G., Lee, S.F., Huang, S.H., Chang, H.W., Chuang, T.M., Liou, Y., Yao, Y.D., Hwu, Y.: Coexistence of ferromagnetism and high-temperature superconductivity in Dy-Doped BiPbSrCaCuO. Surf. Rev. Lett. **9**, 1109–1112 (2002)

17. Zelati, A., Amirabadizadeh, A., Kompany, A., Salamati, H., Sonier Manufacture, J.E.: Characterization of Dy_2O_3 nanoparticles via X-ray diffraction, TEM and PL. Indian J. Inf. Sci. Technol. **6**(12), 5552–5558 (2013)

18. Zelati, A., Amirabadizadeh, A., Kompany, A., Salamati, H., Sonier, J.E.: Effect of Eu2O3 nanoparticles addition on structural and superconducting properties of BSCCO. J. Supercond. Nov. Magn. **27**, 1369–1327 (2014). doi:10.1007/s10948-013-2475-y

19. Mawassi, R., Marhaba, S., Roumié, M., Awad, R., Korek, M., Hassan, I.: Improvement of superconducting parameters of $Bi_{1.8}Pb_{0.4}Sr_2Ca_2Cu_3O_{10+\delta}$ added with nano-Ag. J. Supercond. Nov. Magn. (2013). doi:10.1007/s10948-013-2408-9

20. Kong, W., Abd-Shukor, R.: Enhanced electrical transport properties of nano $NiFe_2O_4$ added $(Bi_{1.6}Pb_{0.4})Sr_2Ca_2Cu_3O_{10}$ superconductor. J. Supercond. Nov. Magn. **23**, 257–263 (2010)

21. Agail, A., Abd-Shukor, R.: Transport current density of $(Bi_{1.6}Pb_{0.4})Sr_2Ca_2Cu_3O_{10}$ superconductor added with different nano-sized ZnO. Appl. Phys. A Mater. Sci. **112**, 501–506 (2013)

22. Mao, C., Zhou, L., Wu, X., Sun, X.: The combination of the polymeric solution-sol-gel process and combustion synthesis to manufacture BiPbSrCaCuO powder. Supercond. Sci. Technol. **9**, 994–1000 (1996)

23. Tampieri, A., Celotti, G., Lesca, S., Bezzi, G., La Torretta, T.M.G., Magnani, G.: Bi(Pb)-Sr-Ca-Cu-O (2223) superconductor prepared by improved sol-gel technique. J. Eur. Ceram. Soc. **20**, 119–126 (2000)

24. Halim, S.A., Khawaldeh, S.A., Mohamed, S.B., Azhan, H.: Superconducting properties of $Bi_{2-x}Pb_xSr_2Ca_2Cu_3O_y$ system derived via sol-gel and solid state routes. Mater. Chem. Phys. **61**, 251–259 (1999)

25. Saleh, S.A.: Studies on sintering effect on the structural and transport properties of (2223) phase. Phys. C **444**, 40–44 (2006)

26. Kocabas, K., Ciftcioglu, M.: The effect of Sb substitution of Cu in $Bi_{1.7}Pb_{0.3}Sr_2Ca_2Cu_{3-x}Sb_xO_y$ superconductors. Phys. Stat. Sol. (a) **177**, 539–545 (2000)

27. Bilgili, O., Selamet, Y., Kocabas, K.: Effects of Li substitution in Bi-2223 superconductors. J. Supercond. Nov. Magn. **21**, 439–449 (2008)

28. Ghazanfaria, N., Kilic, A., Gencerb, A., Ozkana, H.: Effects of Nb_2O_5 addition on superconducting properties of BSCCO. Solid State Commun. **44**, 210–214 (2007)

29. Bean, C.P.: Magnetization of high-field superconductors. Rev. Modern Phys. **36**, 31–39 (1964)